Wang, F., Lühr, H., Xiong, C., Zhou, Y. (2022): Improved Field-Aligned Current and Radial Current Estimates at Low and Middle Latitudes Deduced by the Swarm Dual-Spacecraft. - Journal of Geophysical Research: Space Physics, 127, 6, e2022JA030396.

https://doi.org/10.1029/2022JA030396

JGR Space Physics

RESEARCH ARTICLE
10.1029/2022JA030396

Improved Field-Aligned Current and Radial Current Estimates at Low and Middle Latitudes Deduced by the Swarm Dual-Spacecraft

Fengjue Wang[1], Hermann Lühr[2], Chao Xiong[1,3], and Yunliang Zhou[1]

[1]Department of Space Physics, School of Electronic Information, Wuhan University, Wuhan, China, [2]Geomagnetism, GFZ German Research Centre for Geosciences, Section 2.3, Potsdam, Germany, [3]Hubei Luojia Laboratory, Wuhan, China

Key Points:

- The amplitudes of interhemispheric FACs from single-satellite amount only to about 70% of those from dual-SC due to ignored magnetic field By component
- We interpret the tidal-signature of ionospheric radial currents (IRCs) from single-satellite is spurious, as being due to contributions to the ΔBy component from the equatorial electrojet
- The dual-SC derived IRCs show notable differences at low and middle latitudes between ascending and descending orbital arcs

Correspondence to:

C. Xiong and Y. Zhou,
xiongchao@whu.edu.cn;
zhouyl@whu.edu.cn

Citation:

Wang, F., Lühr, H., Xiong, C., & Zhou, Y. (2022). Improved field-aligned current and radial current estimates at low and middle latitudes deduced by the Swarm dual-spacecraft. *Journal of Geophysical Research: Space Physics*, *127*, e2022JA030396. https://doi.org/10.1029/2022JA030396

Received 15 FEB 2022
Accepted 31 MAY 2022

Abstract Ionospheric currents have widely been investigated by using magnetic measurements from low-Earth orbiting satellites. However, the assumptions of deriving currents from the magnetic measurements have not always been well considered. In this study we performed a detailed analysis of the ionospheric radial current (IRC) and inter-hemispheric field-aligned current (IHFAC) estimates at equatorial and low latitudes derived from the single-satellite and dual-spacecraft (dual-SC) approaches of European Space Agency (ESA's) Swarm constellation. Data considered cover a 5-year period, from 17 April 2014 to 16 April 2019. We found for most of the cases, the IRCs and IHFACs derived from both approaches show consistent latitudinal profiles. However, there are several cases with discrepancy exceeding 5 nA/m^2 between two approaches. On average, the diurnal variations of IHFACs from both approaches agree well with each other for all seasons. But the amplitudes of single-satellite results reach only about 70% of those from the dual-SC. This difference is attributed to the fact that only the magnetic field *By* component is utilized in the single-satellite approach, while both *Bx* and *By* components are considered in the dual-SC approach. Above the magnetic equator, the IRCs derived from single-satellite approach show clear tidal signatures, while such signature cannot be found in the IRCs from dual-SC approach. We interpret these tidal-signature of IRCs as spurious results, caused by equatorial electrojet contributions to the ΔB_y component. The dual-SC derived IRCs show notable differences between ascending and descending orbits. Such differences might be due to a violation of the assumed perfect calibration of Swarm A and C. We suggest a systematic spacecraft-fixed bias in the along-track magnetic field component (*Bx*) between Swarm A and C. By interpreting the IRC differences, we obtain bias values of Δ*Bx* reaching 1 nT. Our results reveal that ionospheric currents are better characterized by the dual-SC approach. But comparison with single-satellite current estimates can help to identify weakness.

1. Introduction

Electric currents in the ionosphere play an important role in the dynamics of the upper atmosphere. Due to the anisotropy of the ionospheric conductivity, there are three different types, Hall, Pedersen, and field-aligned currents (FACs) showing markedly different characteristics dependent on altitude. The Hall current is only prominent in the dynamo region of the E-layer. The Pedersen currents also peak in the E-region but decay gradually toward the F-region. Quite differently, prominent FACs are observed at all altitudes; due to the high conductivity along magnetic field lines they surmount the former by several decades. Therefore, these currents play a dominating role in the F-region and above.

For the determination of electric currents in space, commonly magnetic field measurements taken by satellites are used. For a remote estimation of currents often the Biot-Savart law is used. Conversely, for studying current sheets that are traversed, Ampère's law is typically utilized. Generally, it is not possible to determine uniquely the current from a single magnetic field measurement. Assumptions have to be made about the geometry of the current and their temporal behavior (e.g., Lühr et al., 2020).

Constellation mission Swarm of European Space Agency (ESA) provides several possibilities for estimating current intensities from the magnetic field measurements. Here we focus on the cases where the satellites cross the current layer. Favorable constellations exist when two or even all three spacecraft cross the current region in a close formation. In those cases, Ampère's law in integral form can be used.

$$j = \frac{1}{\mu_0 A} \oint \boldsymbol{B}\, d\boldsymbol{l} \tag{1}$$

where $\boldsymbol{l}$ is a pass element along a closed contour, $\boldsymbol{B}$ is the magnetic field caused by the current, μ_0 the permeability of free space, A is the area encircled by the contour, and j is the mean density of the current passing through this area. For obtaining reliable results, the size of the loop has to be smaller than the scale of the current filament.

For determining the full current vector, magnetic field measurements from at least four well-distributed spacecraft are required, as provided by the Cluster or the Magnetospheric Multiscale mission. From those readings the ring integrals in four planes can be computed. This provides enough information for deriving the current vector and allows in addition to offer information on the uncertainty of the estimates.

In the case of Swarm, current estimates from one, two, or three satellites have been performed. Dunlop et al. (2015) provided comparisons between those solutions. During time of favorable spacecraft configuration, reasonable agreements are achieved between the different approaches. Here, within this study we limit our attention to current determination by two or even one Swarm spacecraft. One such example is the estimation of zonal currents in the F-region. Lühr et al. (2016) made use of the satellites, Swarm A and Swarm B, which flew at different altitudes (470 and 520 km, respectively) on their polar orbits. During the months February–June 2014 the orbital planes were sufficiently close together that the zonal current densities passing through the loop in the vertical plane, confined by the altitudes of the two orbits, could be determined. Obtained average current densities at middle and low latitudes are about 20 nA/m^2, flowing predominantly eastward on the dayside and westward on the nightside with about 10 nA/m^2.

More important is the estimation of the vertical current component. The Swarm satellite constellation is deliberately maintained such that suitable magnetic field measurements for this purpose can be obtained throughout the mission. Swarm A and C fly side-by-side, separated only by 1.4° in longitude. By considering two magnetic field readings, separated by 5 s in along-track direction, from both spacecraft a rather regular quad of readings is obtained. These are the basis for the ring integral approach according to the Ampère's law. In this way the mean vertical current density crossing the area, outlined by the quad of measurements, is derived. More detailed descriptions of the Swarm dual-spacecraft current (dual-SC) estimates have been given by Ritter et al. (2013) and Lühr et al. (2020).

A prime requirement for all the multi-spacecraft current estimate methods is a precise calibration of the magnetometers on board the satellites. Any bias of the magnetic field readings on one spacecraft with respect to the others will cause errors in the current estimates. In the case of Swarm highly precise instruments are on board, both vector field and scalar magnetic field. These provide ideal conditions for reliable current estimates. Unfortunately, it was discovered after launch that disturbance fields with typical amplitudes of 5 nT sometimes can occur (Brauer et al., 2018). These are caused by thermoelectric currents flowing through the grounding straps when the sun is shining on the thermal blanket around the Vector Field Magnetometer (VFM). Depending on the solar aspect angle, spurious magnetic fields with different amplitudes and directions are generated. Later on, it was discovered that also the readings of the Absolute Scalar Magnetometer (ASM) are somewhat affected by thermomagnetic currents (e.g., Jager et al., 2016). More detailed descriptions of these thermomagnetic disturbances and the strategies to correct for the effects are given by (Tøffner-Clausen et al., 2016).

The task of calibrating the vector magnetic field data during the mission became even more complicated after 5 November 2014 when the ASM on Swarm C permanently failed. The total field values from the ASM are typically used to calibrate routinely the VFM data. After drop-out of ASM on Swarm C the missing total field values had to be estimated from related measurements at the accompanying spacecraft Swarm A. The quality of this correction approach has been checked by De Michelis et al. (2017).

The instrumental effects, described above, may lead to errors in the derived vertical current density based on the dual-spacecraft approach. It is the purpose of this study to characterize the uncertainty of the Swarm current estimates. This has never been done in any systematic way. The datasets we use are the current density values from the first 5 years of the Swarm mission, and considering the vertical and the FAC components. For an assessment we compare the current densities derived by the single-satellite approach with those from the dual-spacecraft method. It is well-know that the single-satellite current estimates have their limitations, but they are not affected by the absolute calibration of the magnetometers on the two Swarm spacecraft. Here we focus our attention on middle and low latitudes where currents in the F-region are rather small. Therefore, deficits in calibration of the

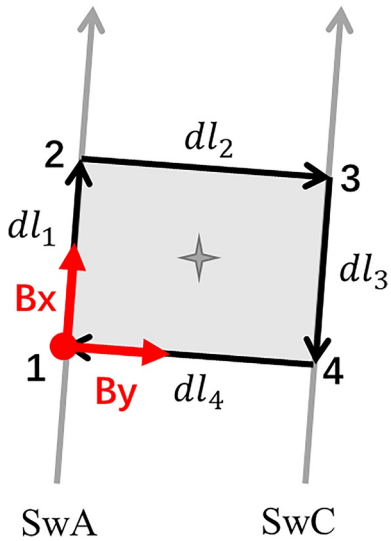

Figure 1. A diagram of an integral loop with the four measuring points used to estimate the average current density passing through the enclosed area. The *Bx* component is aligned with the flight direction, *By* points from Swarm A to Swarm C, and *Bz* completes the triad pointing downward.

magnetometers on Swarm should be more evident than at auroral latitudes where much stronger field-aligned currents are flowing.

In the sections to follow we will first present the datasets utilized in this study and also outline the basic processing steps that have been applied to the magnetic field data. In Section 3, examples and systematic comparisons are presented of vertical currents and FACs derived by the single and dual-SC approaches at equatorial and low latitudes. Possible reasons for appearing discrepancies between the two approaches are discussed in Section 4. Finally, the main findings are summarized in Section 5.

2. Data and Processing Approaches

2.1. Swarm Satellites and FAC Products

ESA's Earth observation mission Swarm was launched on 22 November 2013. It consists of three identical satellites in near-polar orbits (inclination about 87.5°) at different altitudes. In the final constellation, Swarm A and C fly side-by-side at about 450 km altitude, with a separation of 1.4° in longitude, while Swarm B flies around 60 km higher. Each of the three satellites is equipped with a set of six instruments (Friis-Christensen et al., 2008). In this study, we use mainly the magnetic field vector data, sampled by the fluxgate VFM. The vector data are calibrated against the ASM, a Helium vapor instrument. This procedure ensures in principle high absolute accuracy of the independent data sets from the three spacecraft.

As part of the Swarm mission support, ESA is conducting a number of standard data processing tasks. Among them the preprocessing of the magnetic field measurements is an important task. These data are partly further processed for generating useful Swarm Level 2 products. We take advantage of the Level 2 product "FAC" that includes estimates of the field-aligned currents, FAC, and the ionospheric radial current component, ionospheric radial current (IRC). Both these products are derived individually from the three Swarm spacecraft measurements and also by the combination of the Swarm A and C magnetic field data. The various datasets are freely available from the ESA website at https://swarm-diss.eo.esa.int. We made use of the Level-2 FAC data with product identifier "_FACXTMS_" of 1 Hz time resolution (version 03).

2.2. FAC Derived From Dual and Single Satellites

For this study we considered the current estimates for the period from 17 April 2014 to 16 April 2019. The start date is determined by the completion of the Swarm satellite constellation. The considered 5 years of data just provide an equal distribution of local time sampling over all four seasons. Since the lower pair spacecraft need about 131 days for sampling the 24 hr of local time, within 5 years all local times are covered 14 times during each season.

In practice, two magnetic field measurements are taken along the track, 5 s separated, by both satellites, in order to obtain 4 readings, forming a symmetric quad, see Figure 1. The connected four points represent the closed integral loop, as illustrated in Figure 1. Since all the measurements are in a horizontal plane, we derive the average vertical current density, j_z, passing through the encircled area. In practice, the integration is replaced by a discrete summation of the B-field components at the corners.

$$j_z = \frac{2}{\mu_0 A}\left[\left(B_{x_{t1}} + B_{x_{t2}}\right) dl_1 + \left(B_{y_{t1}} + B_{y_{t2}}\right) dl_2 - \left(B_{x_{t3}} + B_{x_{t4}}\right) dl_3 - \left(B_{y_{t4}} + B_{y_{t1}}\right) dl_4\right] \quad (2)$$

where A is four times the area encircled by the contour, μ_0 is the permeability of free space, $B_{x,tn}$ and $B_{y,tn}$ are the horizontal components aligned with the connecting lines; dl_n are the line elements between the corners, and $A = (dl_1 + dl_3)(dl_2 + dl_4)$.

Underlying assumptions are that currents are constant over the period of 5 s, the time used for taking the two samples, and that the spatial scale of the current structure (half the wavelength) is larger than size of the quad. It is known that the small-scale current structures are very variable, therefore the magnetic field readings are first low-pass filtered with a cut-off period of 20 s before current estimation. This procedure suppresses the short-term variations and provides an along-track averaging over a 150 km wavelength, thus, satisfying both assumptions.

An estimate of the field-aligned current is derived by mapping the vertical current component onto the ambient magnetic field direction. The flow direction is the same as the *B*-field, from the southern to the northern hemisphere. This procedure of FAC estimates becomes progressively more uncertain toward lower latitudes. Therefore, no such currents are provided within the range of ±15° magnetic latitude (MLat), where the angle between the vertical current and the field line exceeds 60°. Detailed descriptions of the dual-SC current estimations are provided by Ritter et al. (2013) and Lühr et al. (2020).

The other Swarm data product considered here is the vertical current density derived separately from each spacecraft measurements. In that case a reduced form of Ampère's law is employed

$$j_z = \frac{1}{\mu_0}\frac{1}{v_x}\frac{\Delta B_y}{\Delta t} \tag{3}$$

here v_x is the along-track velocity component, ΔB_y is the field variation in the horizontal plane and perpendicular to the field flight direction, primarily in east-west, and Δt is the time step of samplings, here 1 s. For obtaining reliable results, important assumptions have to be fulfilled: (a) the recorded ΔB_y variations represent spatial gradients (not temporal variations); (b) ΔB_y is caused entirely by the current traversed (not by external sources); (c) the traversed currents are organized in elongated sheets perpendicular to the flight direction. For mitigating assumption (a) we have low-pass filtered the data with a cut-off period of 20 s in order to suppresses the short-term variations. More details of the processing steps are given by Ritter et al. (2013). The other two assumptions should be kept in mind during the discussion of the derived differences between single and dual-SC current estimates.

3. Results

3.1. Examples of Field-Aligned Currents and Radial Ionospheric Currents

As described in the previous section, the Swarm Level-2 product "FAC_TMS_2F" contains FACs and IRCs, both derived individually from each Swarm spacecraft and from the combination of the Swarm A/C pair. Before studying the statistical properties of these current components at middle and low latitudes in more details, we introduce a few examples. The features found here may help to understand later the mean properties.

Figure 2 shows in the left half FAC estimates from 1 May 2014. As mentioned before, there are no FAC values provided for latitudes below 15° MLat because of the low magnetic inclination near the equator. The individual curves from the two satellites, Swarm A and C, show a lot of small-scale variations. This signal is partly uncorrelated between the two spacecraft although the 1-Hz FAC readings have been low-pass filtered with a 20-s cut-off period (corresponding to a wavelength of 150 km). This implies that the two spacecraft partly cross different smaller scale FAC sheets. Conversely, the black curve resulting from Ampère's ring integral approach is clearly smoother. Even though, the larger scale FAC variations agree fairly well between the single and the dual-SC FAC estimates. This provides confidence in the two independently calculated current components.

The data in the left side panels of Figure 2 have been obtained in the sector shortly after noon (12:12 and 12:17 MLT), and in both hemispheres we find similar latitudinal FAC profiles. This suggests that at the time of passage the interhemispheric FACs (IHFACs) dominate the large-scale current distribution.

The right panels of Figure 2, from 13 April 2019, show currents from a time sector around dawn. Here the observed FAC density are much smaller, than the amplitudes in the first example. The single-satellite results show again many details of small-scale FACs, but the gross features are also captured by the dual-SC curves. However, we observe a bias with opposite signs in the northern and southern hemispheres between the two types of FAC estimates. This implies that at least one of the two approaches suffers some problems. From the opposite signs of

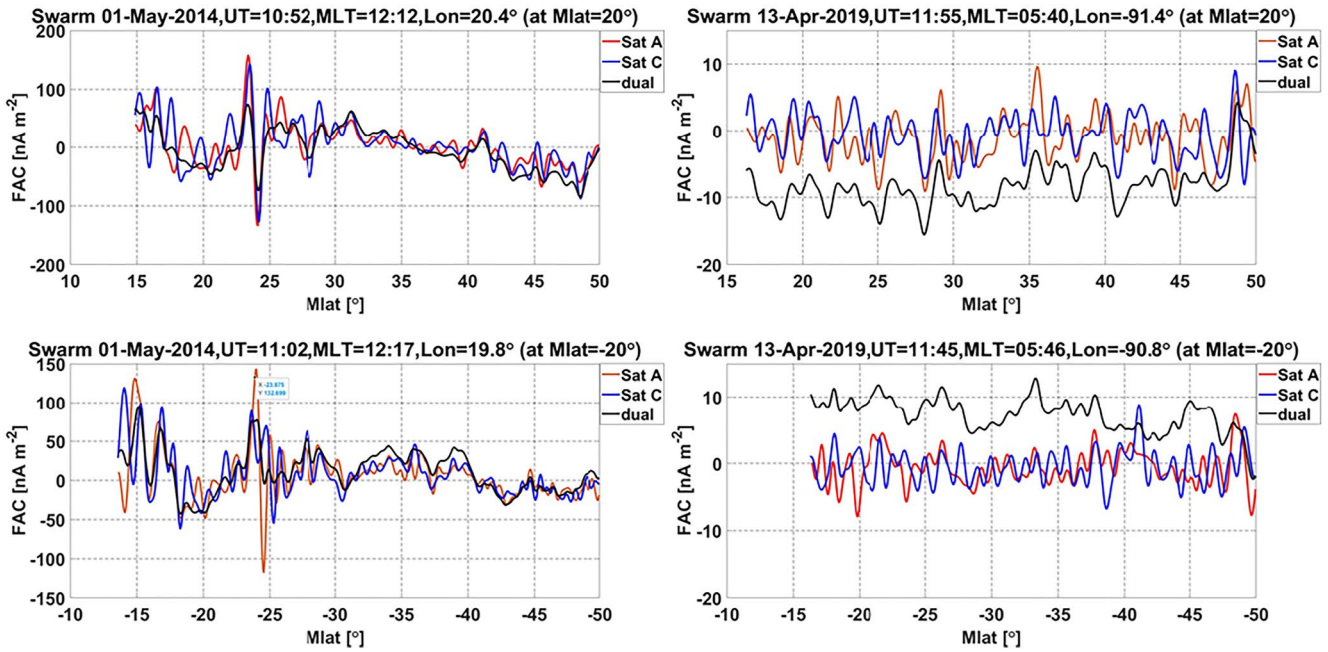

Figure 2. Examples of field-aligned current profiles along geomagnetic latitude at noon and night in both hemispheres. The red, blue and black lines represent the results from Swarm A, Swarm C and Swarm A&C respectively. Positive values reflect currents from south to north.

the mean current densities in the two hemispheres we can also conclude that the dual-SC approach returns upward flowing currents at all latitudes, while the single-satellite results indicate very weak currents.

At low and equatorial latitudes only IRCs are estimated. Figure 3 shows these current components for the same examples in the latitude range from −15° to 15° MLat. For the 1 May case (around noontime) we find again a good match between single and dual-SC IRC results. Current density becomes really small around the magnetic equator. Toward higher latitudes the current strength increases, indicating upward currents in the southern hemisphere and downward in the northern hemisphere. Both these mark the latitudinal region where the south-to-north IHFACs start, which are quite obvious in the example shown in the left panels of Figure 2.

The right frame of Figure 3 presents the low-latitude IRC from 13 April around dawn. For this time of the day only weak currents are expected. This inference is well supported by the single-satellite IRC results. Conversely, the dual-SC results suggest a significant upward current. This questionable notion can also be found at higher latitudes, as seen in the right panels of Figure 2.

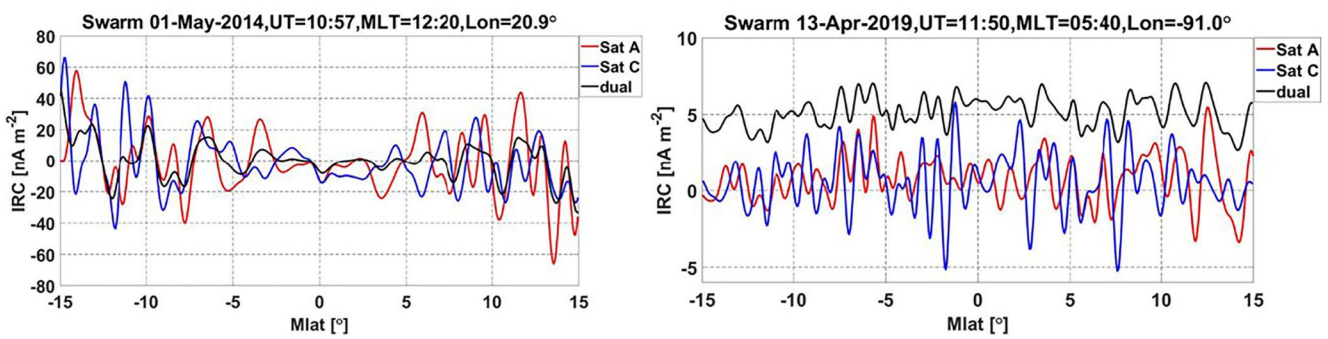

Figure 3. Examples of vertical current profiles along geomagnetic latitude at noon and night. Positive values reflect upward currents.

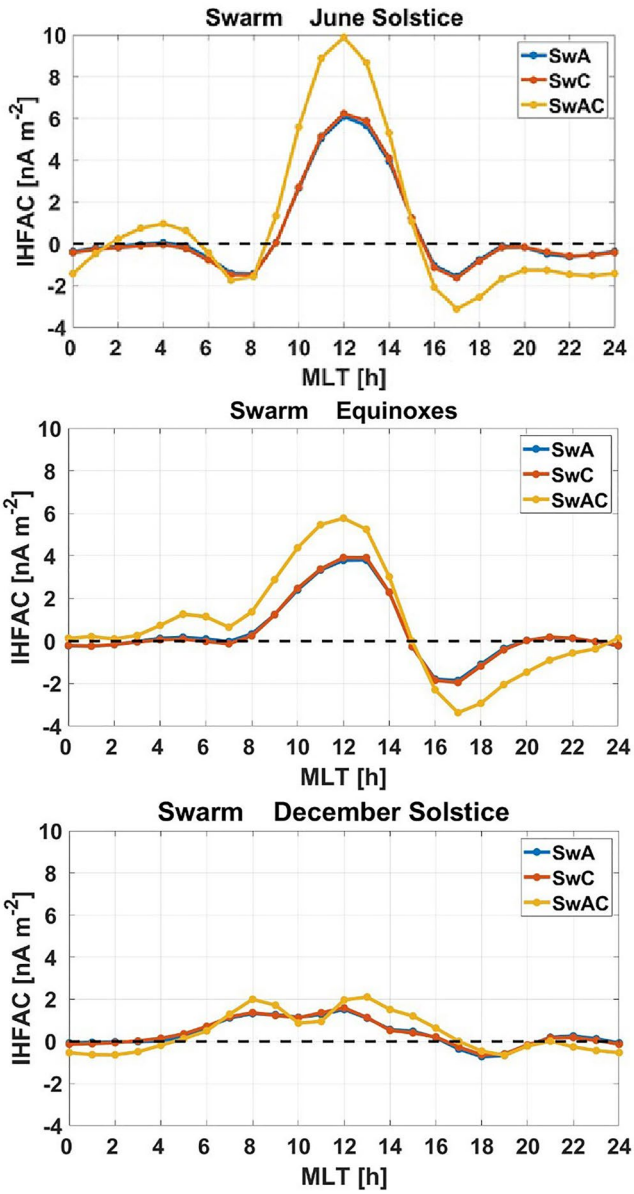

Figure 4. Comparison of average local time dependence of the low-latitude inter-hemispheric field-aligned currents derived from Swarm A(blue), Swarm C(red) and Swarm A&C(yellow) separately for the three Lloyd seasons. Positive value represents currents from the south to north.

3.2. Comparison of IHFACs From Single and Dual-SC Estimates

After having seen the details of FACs at middle and low latitudes we are now interested in the systematic characteristics. One assumption is, that the whole derived vertical current density is caused by FACs. Such an assumption is probably justified inside the auroral region but is not true at middle and low latitudes. Therefore, we make use of the current continuity condition. In this study we thus require that the intensity of IHFACs is the same in both hemispheres at the conjugate locations. This is obtained by deriving the symmetric part, $(FAC_{north} + FAC_{south})/2$, which is considered in the following as IHFAC. The latitude range for this analysis is limited at the lower end at 15° MLat and at the higher end at 35° MLat. The lower limit is dictated by geomagnetic field geometry and the upper limit by the change in IHFAC characteristic as described by Park et al. (2020). The FAC estimates from both the single and dual-SC processing were treated exactly in the same way, in order to identify possible systematic differences.

We are aware of the fact the Swarm satellites do not sample, in general, the same magnetic longitudes (MLon) on their mid-latitude passes. Therefore, our FAC averages from the two hemispheres do not always come from the same magnetic longitude. However, it can be assumed that the correlation length of FAC sheets is longer in longitudinal direction than in latitude. We verified that by an alternative statistical approach, sorting the FAC readings into MLat versus MLon bins and computed the IHFAC from the mean values of the truly conjugate bins in the two hemispheres. This provided practically the same results as our averages of the orbit-by-orbit IHFAC estimates.

In the beginning we averaged the derived IHFAC values over all longitudes and the considered latitude range for retrieving the mean diurnal variation. Figure 4 shows the dependence of the IHFAC density on local time, separately for the three Lloyd seasons (June solstice: May-Aug.; Equinoxes: Mar., Apr., Sep., Oct.; December solstice: Nov.-Feb.). Positive values represent currents from the southern to the northern hemisphere. The orange curves, representing the dual-SC results, reproduce very well the IHFAC diurnal variation reported by Lühr et al. (2019) (see their Figure 2). The two single satellite results from Swarm A and C give undistinguishable diurnal variation curves (blue and red). This is expected due to their small spatial separation. For all seasons the two processing approaches result in very similar IHFAC diurnal variation, but the dual-SC amplitudes are larger approximately by a factor of 1.5. This is an indication that part of the mid-latitude FAC signal is missed by the simple single-satellite approach.

After having seen the mean diurnal variation, we are now interested in more details concerning the IHFAC distribution. From Figure 4 we can conclude that the curves for June solstice and Equinoxes look quite similar while that for December solstice differs a lot. Already Park et al. (2011) noted that IHFACs are better ordered by two seasons. We follow that advise and sort the data for all following analyses into the summer (May-Oct.) and winter (Dec.-Mar.) seasons. Figure 5 presents for these two seasons the MLat versus geographic longitude (GLon) distribution of the IHFAC density for the 4 hours around noon (10:00–13:00 MLT), when the amplitudes are largest. Only the northern latitudes are presented because, by definition, the values are the same in the southern hemisphere. Since a prime aim of our study is the validation of the IHFAC estimates, here again results from the single and dual-SC current processing are shown. From Figure 4 it is known that two spacecraft, Swarm A and C, give on average the same results, therefore we show for comparison only results from Swarm A for representing the single-satellite IHFAC values.

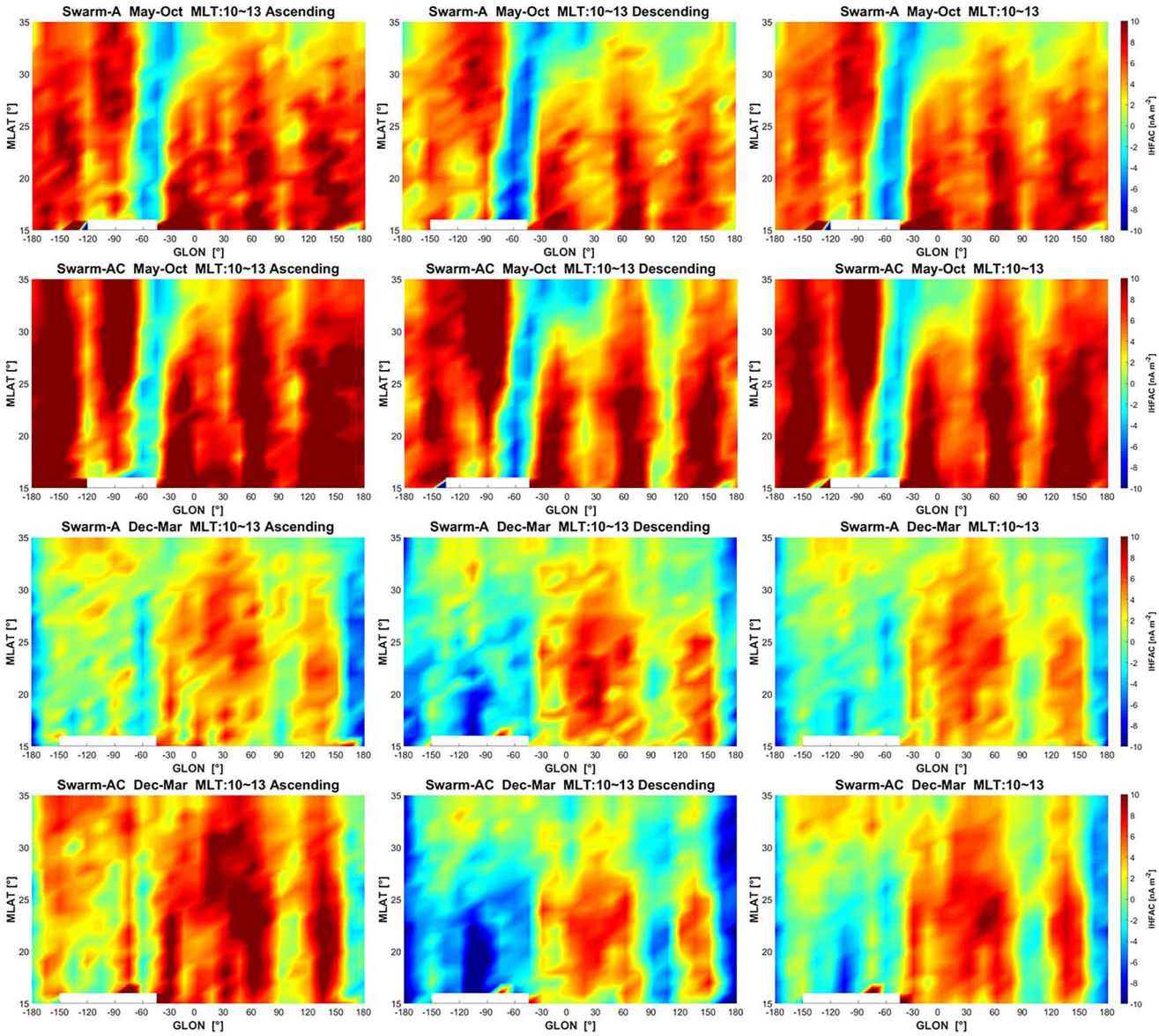

Figure 5. Magnetic latitude versus longitude distributions of the inter-hemispheric field-aligned current (IHFAC) derived from ascending (left), descending (middle) and all orbits (right) around noon (10 MLT–13 MLT) for Swarm A and Swarm A&C in the two seasons (May–Oct and Dec–Mar). Positive value represents currents from the south to north.

There are three panels in each row of Figure 5. They present from left to right the IHFAC densities derived from ascending, descending, and all orbits. We start with the summer season. Here the differences between results from ascending and descending arcs are not so prominent. Also the longitude patterns are very similar between single and dual-SC current estimates. Just the amplitudes are larger from the dual-SC approach, consistent with the results shown in Figure 4. Quite prominent is the longitudinal stripe near −60°E GLon of negative currents. This reverse IHFAC flow occurs in the region of the South Atlantic Anomaly (SAA) and has earlier been noted and described (e.g., Lühr et al., 2019; Park et al., 2011). Otherwise, the longitudinal distribution is dominated by enhanced activity bands separated by about 90° GLon. We will come back to this feature further down in the context of Figure 6.

The lower half of Figure 5 presents the IHFAC distribution during our winter season. Here we find clear differences between the longitudinal distributions from ascending and descending passes. For example, the descending

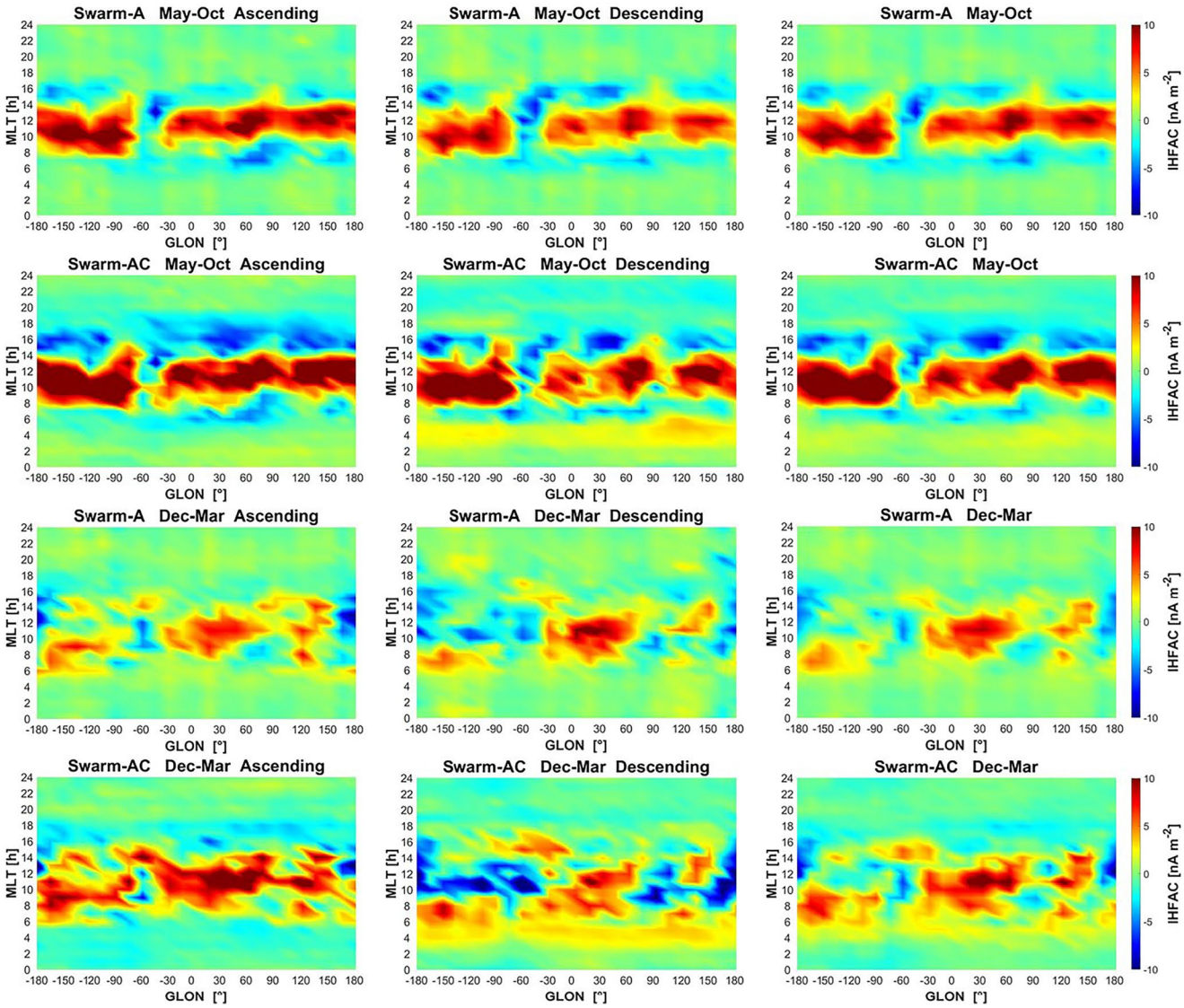

Figure 6. Magnetic local time versus longitude distributions of average inter-hemispheric field-aligned current (IHFAC) over 15°Mlat ~35° Mlat derived from ascending (left), descending (middle) and all orbits (right) for Swarm A and Swarm A&C during the two seasons (May–Oct and Dec–Mar). Positive value represents currents from the south to north.

passes are dominated in the western half by north-to-south IHFACs, while opposite current flows prevail at eastern longitudes. Conversely, the ascending passes do not show such a clear longitudinal sectoring. Here we find a longitudinal pattern similar to that of the ascending orbits in the summer season. For explaining these differences in IHFAC winter patterns we have to realizes that the noon-time data for the ascending and descending passes come from different years. It has been noted earlier that the IHFAC pattern is significantly influenced by the effect of the stratospheric sudden warming (SSW) events (e.g., Lühr et al., 2019). Depending on the intensity of the SSW event and the moon phase at which the noontime data are sampled the IHFAC patterns will vary from year to year. The convincing thing in our case is that the differences in longitudinal variations are returned from both the single and dual-SC IHFAC estimates. This provides confidence into the derived FAC densities.

From Figure 5 we can deduce that the intensity of IHFAC does not vary much over latitude within the considered range, 15°–35° MLat. Therefore, it is justified to make use of the averages over latitude. For a further analysis we consider these averages and plot them in frames of magnetic local time (MLT) versus longitude (GLon). Figure 6 provides a good overview of the IHFAC diurnal variation and how it varies with longitude. Here again

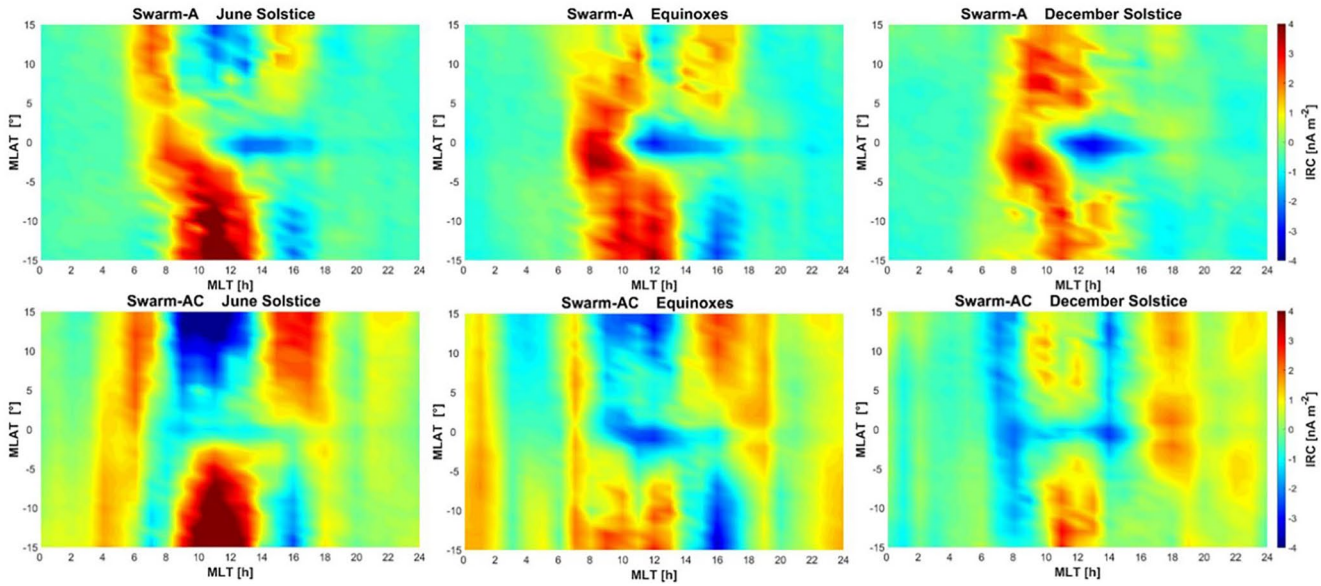

Figure 7. Magnetic latitude versus magnetic local time distributions of the ionospheric radial current (IRC) derived from Swarm A (top) and Swarm A&C (bottom), separately for the three Lloyd seasons. Positive values reflect upward currents.

the marked differences between the summer and winter seasons are obvious. During summer the prominent northward IHFAC around noon is outstanding. While around morning and evening hours southward currents are prevailing. Conversely, for winter conditions no clear diurnal variation pattern is observable. This type of presentation, local time versus longitude, is suitable for visualizing solar tidal signatures. During the summer season clear indications of IHFAC density peaks appear around noon, separated by about 90° in longitude. The series is somewhat disturbed by the minimum around −60°E GLon (SAA region). It is interesting to note that the tidal features are confined to the daytime hours from 06 to 18 MLT. The low E-region conductivity at night seems to inhibit the IHFAC activity. In contrast, the IHFAC patterns during our winter months do not reflect clear solar tidal signatures. Those longitudinal patterns seem to be affected by other processes including the SSW.

A promising observation from Figure 6 is that the IHFAC patterns in all the frames are very similar between the single and dual-SC results, just the amplitudes of the dual-SC estimates are, as usually, somewhat larger. There is one exception, during the morning hours, 04 to 06 MLT, small but persistent northward IHFACs appear in the frames of dual-SC results from descending arcs of both seasons. Such features are not visible in neither the single-satellite estimates nor in dual-SC results from ascending arcs. This fact strongly suggest that these early-morning currents are an artifact. We will revisit such features in Section 4.

3.3. Comparison of IRCs From Single and Dual-SC Estimates

As introduced above in the low-latitude range, ±15° MLat, no FACs are estimated. Here just the radial current component is determined. Also for that, we want to check the validity of the single and dual-SC estimates. Figure 7 shows the current densities in latitude versus local time frames, as derived by the two techniques separately for the three Lloyd seasons. It is obvious, that the dual-SC results in the bottom row reproduce well the results presented in Figure 5 of Lühr et al. (2019). This is no surprise, since both studies are based on Swarm magnetic field data. At latitudes beyond ±10° MLat we find typically IRCs with opposite polarities on the dayside. These are interpreted as parts of the IHFAC systems. Right above the magnetic equator the mean current density is low, but is directed systematically downward around noon and upward during the evening hours. This is related to the wind-driven F-region current generator as earlier proposed by Rishbeth (1971).

However, when comparing with the IRC densities from Swarm A, marked differences appear between the two calculation approaches, especially close to the magnetic equator. For finding possible explanations, we took a closer look at the IRC longitudinal distribution for the hours around noontime. Figure 8 presents a comparison

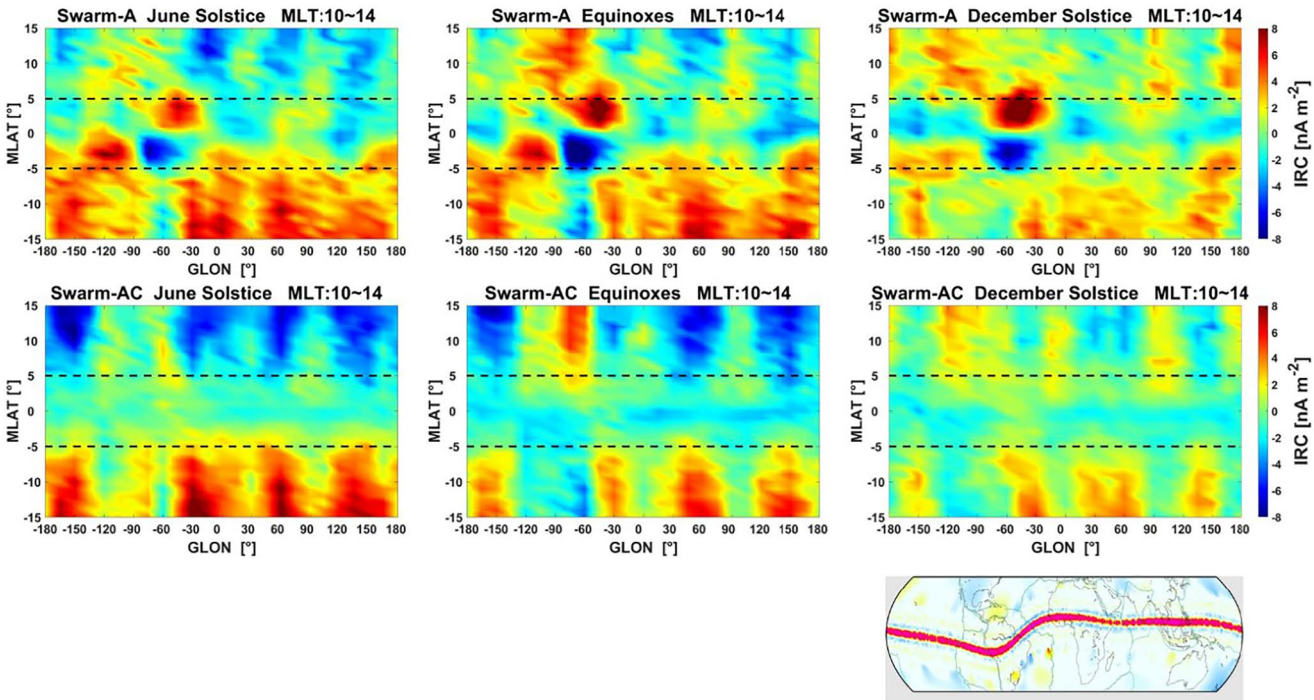

Figure 8. Magnetic latitude versus longitude distributions of the ionospheric radial current (IRC) derived from Swarm A (top) and Swarm A&C (bottom) around noontime (10 MLT ∼ 14 MLT), separately for the three Lloyd seasons. The thick red line in the global map (right bottom panel) represents the equatorial electrojet distribution. Positive values reflect upward currents.

between single and dual-SC IRC estimates, separately for the three Lloyd seasons. At latitude ranges beyond ±5° MLat, dashed lines, the results from the two approaches are quite similar. Longitudinal sectors with opposite current directions appear in the two hemispheres. They represent the equatorial ends of the IHFAC system. These patterns are clearer in the dual-SC plots but also discernible, one-to-one, in the current estimates from Swarm A. Opposed to that, completely different IRC distributions result from the single and dual-SC current estimates within the latitude range ±5° MLat. While there are only weak downward currents resulting from dual-SC calculation over the magnetic equator with little longitudinal structure, we find intense current patches derived by the single-satellite approach within the low-latitude band. Peak upward currents appear at all seasons in the northern part and related downward currents in the southern close to −60°E GLon. Opposite current flows, although with smaller amplitude, are found at longitudes west of −90°E GLon. This reversal is clearest in the December solstice frame.

We prefer to interpret these low-latitude radial current features from Swarm A as spurious signals. The equatorial electrojet (EEJ) is flowing along the magnetic equator. It is accompanied by a relatively large magnetic signal at Swarm altitudes (e.g., Alken, 2020). Since the EEJ is flowing predominantly eastward, it mainly causes magnetic deflections of the north-south, B_x component. However, there are longitude sectors, especially over the Atlantic and South America, where the orientation of the current flow deviates significantly from the east-west direction. In those regions the EEJ makes also contributions to the east-west, B_y component. As outlined in Equation 3, the radial current component derived from single-satellite magnetic field readings is based solely on the gradient of the *By* component along the orbit, regardless where this signal comes from, for example, electrojet, ring current, or F-region current. For supporting our claim of EEJ origin of the low-latitude features from Swarm A we added in Figure 8, below the December solstice frames a map with the EEJ (red line). As expected from the orientation of the EEJ, we find intense upward IRC signature in the north and downward currents in the south where the EEJ exhibits a significant northward flow direction, around −60° GLon. The opposite IRC pairs of flow directions are found over longitude regions with southward bearing of the EEJ. And the amplitudes of the apparent IRCs are proportional, as expected, to the deviation angle.

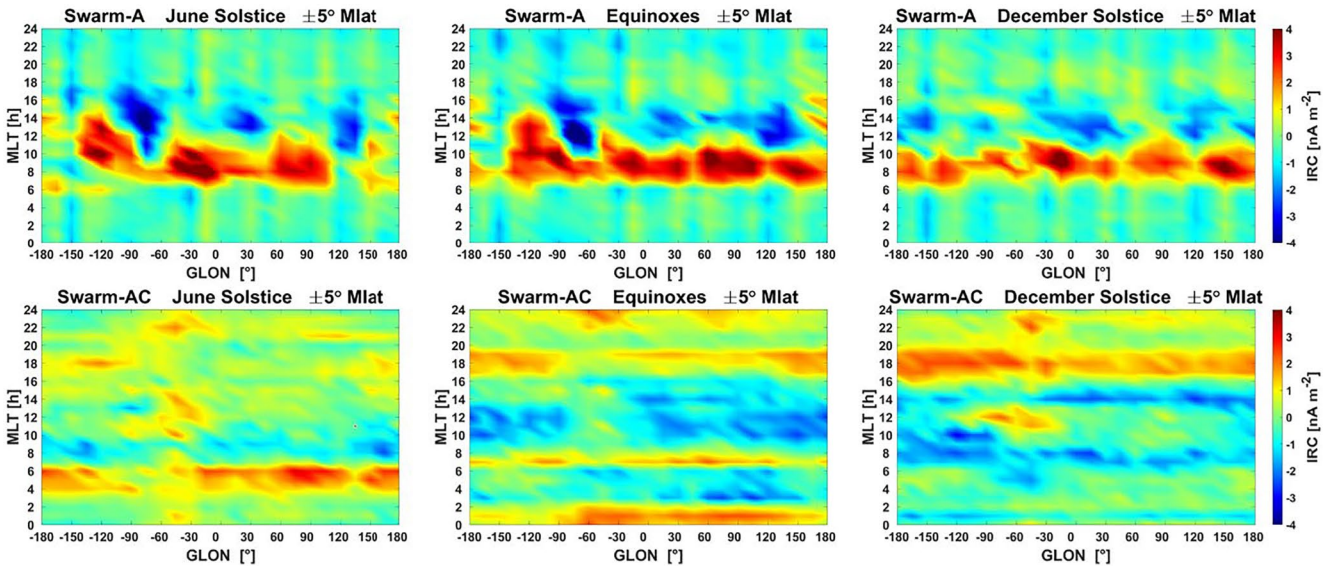

Figure 9. Magnetic local time versus longitude distributions of the average ionospheric radial current (IRC) over the latitude range ±5°Mlat derived from Swarm A (top) and Swarm A&C (bottom), separately for the three Lloyd seasons. Positive values reflect upward currents.

In the case of the dual-SC IRC results the situation is different. Here the magnetic fields from current systems that close outside the integration loop (all scalar magnetic fields) are rejected. Only those currents that pass through the loop contribute to the vertical current estimate. Therefore, no influence of the EEJ is expected in the dual-SC estimates.

For further checking our conclusions on EEJ influence, we present in Figure 9 the local time versus longitude distribution of the IRC averaged over the latitude range ±5° MLat, separately for the three Lloyd seasons. Here again a stark difference between the single and dual-SC IRC estimates appears. As noted before, this kind of presentation is suitable for visualizing solar tidal signatures. The current density patterns from Swarm A clearly repeat most prominent EEJ tidal signatures of the different seasons, wave-3 (DE2) around June solstice, wave-4 (DE3) during equinoxes, and wave-2 (SW4) around December solstices (see Lühr and Manoj (2013) for comparison). Conversely, the dual-SC IRC estimates from low and equatorial latitudes show only little longitudinal variation but no tidal signatures in any of the seasons. This further confirms the limitations of the Swarm single-satellite vertical current estimates near the magnetic equator.

Just for completion, the dual-SC estimates show some, although weak, mainly upward currents during nighttime that find no counterpart in the Swarm A estimates. Possible reason for that will be treated in the Discussion section.

3.4. Differences Between Ascending and Descending Orbit Arcs

Already in Figure 6 we observed some northward IHFACs of dual-SC during early morning hours (04:00–06:00 MLT) in descending orbit arcs, which had no counterparts in ascending arcs, and no such currents appeared in the results from Swarm A. This may be an indication for spurious current signals from dual-SC estimates. For investigating such possibilities in more details, we take a closer look at the radial current distribution (since IRC is the original product) over the full range of ±50° MLat. Figure 10 shows IRC distribution in MLat versus MLT frames. In the left and middle columns the mean current estimates from ascending and descending arcs are shown, respectively. The right column presents half the difference between the two ($(IRC_{Asc} - IRC_{Desc})/2$). We sorted the data again into the two seasons, as defined before for the IHFACs, summer (May–Oct.) and winter (Dec–Mar.).

The top row of Figure 10 shows the summer IRC results from Swarm A, below are the dual-SC estimates presented for the same periods. In general, the single and dual-SC IRCs from the ascending and descending arcs look quite similar during daytime. Also here, the dual-SC estimates show larger amplitudes than the single-satellite

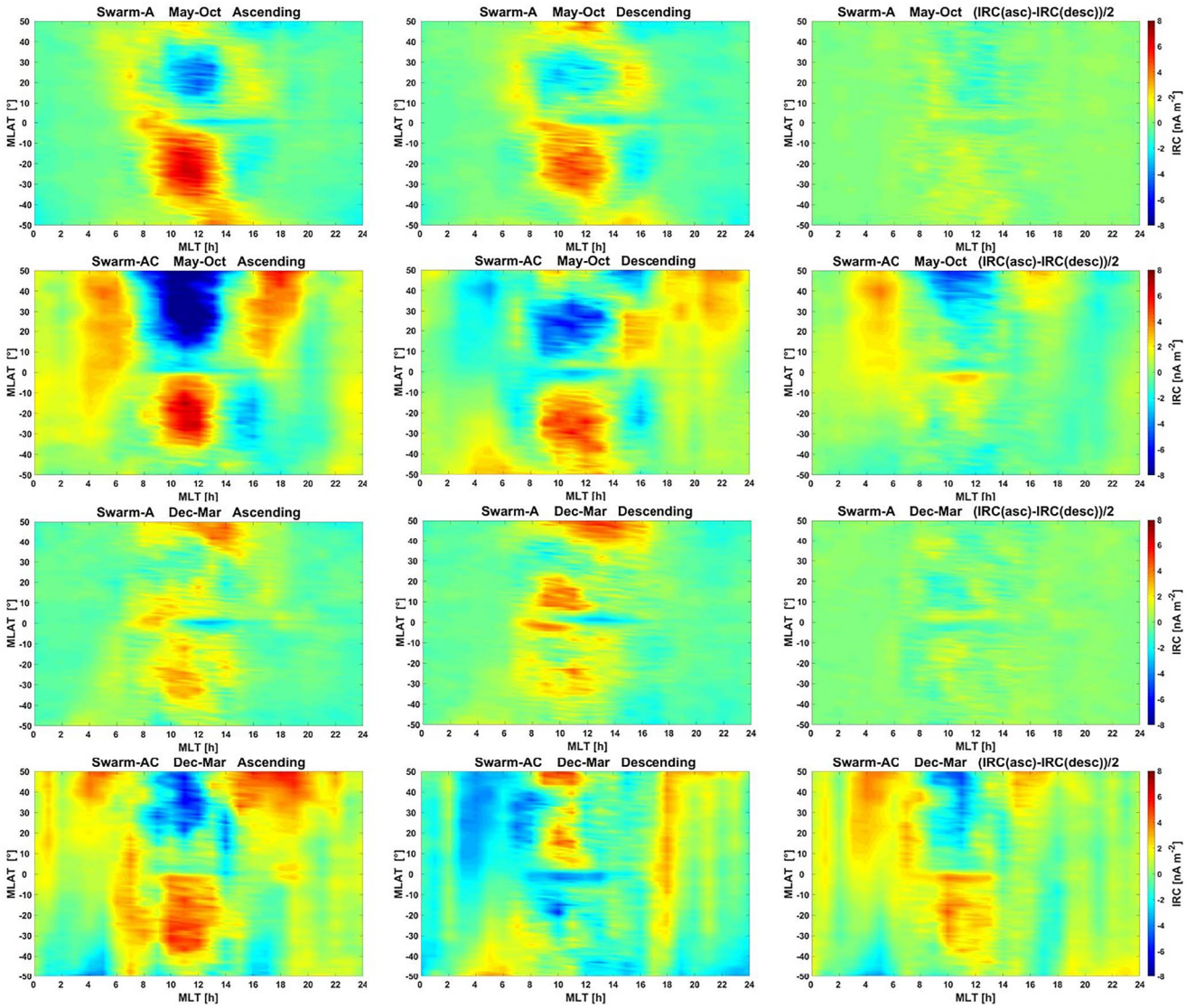

Figure 10. Magnetic latitude versus magnetic local time distributions of the ionospheric radial current (IRC) derived from ascending, descending orbits and difference between the two kinds of orbits, separately for Swarm A and Swarm A&C during the two seasons (May–Oct and Dec–Mar). Positive values reflect upward currents.

approach, as was already noted in earlier sections. During night-time the results from the approaches show more prominent differences. Theoretically, there should not be any differences between the results from ascending and descending arcs. This expectation is largely fulfilled in the case of Swarm A current estimates. In the case of the dual-SC approach persistent features appear. In particular, in the northern hemisphere there are upward directed differences in the morning (04:00–06:00 MLT) and in the evening at higher latitudes. Around noon some downward different currents appear. Generally, difference amplitudes increase toward higher northern latitudes. In the southern hemisphere the differences are much smaller.

For the winter season we find larger differences between the IRCs derived by the single and the dual-SC approaches, both for the ascending and descending arcs (Figure 10, two lower rows). We have no immediate explanation for these. When looking at the differences between estimates from ascending and descending arcs we find again very tiny values from Swarm A but some systematic features from the dual-SC results. In the northern hemisphere there are again the upward directed difference currents in the morning and in the evening and some downward currents around noon at higher latitudes. In the southern hemisphere upward currents around noon are dominating. When discussing these differences, we have to keep in mind that they are generally small, hardly

surmounting 3 nA/m^2. In the next section we will discuss which errors in magnetometer calibration may be responsible for the derived differences.

4. Discussion

The Swarm project provides fully processed constellation-based data products. One of them is the estimation of radial and field-aligned currents. Here we present for the first time a systematic comparison between the estimated IRC and FAC densities from the single and dual-SC approaches. Our aim is to identify weaknesses of the one or the other Swarm processing techniques. As examples, we took a closer look at two phenomena, low-latitude interhemispheric field-aligned currents and vertical currents near the equator.

Important roles for the assessment of reliability play the underlying assumptions and their justification. In the case of FAC estimates from single-satellite B-field measurements, Assumption (3) in Section 2.2 requires that currents are flowing in elongated sheets, which are oriented perpendicular to the flight direction. Any deviation from that, a different angle of attack or a more filamentary current geometries, will cause also signals in ΔB_x. Since only ΔB_y variations are considered in this approach, part of the signal of the actual current density is missed. In Figure 4 we can see that the IHFACs from single-satellites represent well the diurnal variations for all seasons, but the amplitudes amount only to about 70% of those from dual-SC technique. This strongly suggests that IHFACs in general do not satisfy Assumption (3). When looking through individual current density profiles (as those in Figure 2), we do not find systematically larger FAC estimates from the dual-SC method. Rather, the amplitude relation varies from orbit to orbit and from day-to-day. From that we may conclude, the form and orientation of the IHFAC current sheet at middle latitudes is a rather variable feature. The difference we find in Figure 4 is just a mean feature. Further analysis reveals that, apart from the amplitude deficit, IHFACs from single satellite return well the longitudinal and latitudinal (within 15°–35° MLat) distribution (see Figure 5) and the tidal activity patterns (see Figure 6). All this confirms, magnetic field measurements from individual satellites on near-polar orbits can make useful qualitative contributions to the investigation of IHFACs.

We obtain somewhat different results for the latitudes close to the magnetic equator. Here the single-satellite approach returns significantly different current distributions from the dual-SC IRCs (see Figures 7–9). Our explanation for that is the violation of Assumption (2): ΔB_y is caused entirely by the current traversed. We have argued that the different features in IRC from Swarm A are caused by contributions to ΔB_y from the EEJ. This argument is well confirmed by the typical characteristics of the EEJ (e.g., latitudinal variation and solar tidal patterns). From these results it can be concluded that magnetic field measurements from a single satellite are in general not sufficient to reveal the details of the wind-driven F-region currents at the equator. For example, Park et al. (2010) made use of Challenging Minisatellite Payload magnetic field data for resolving details of the F-region currents. Among others, they report a modulation of the vertical current around noon by solar tides, but they found no tidal signals associated with the upward currents in the evening around 18 MLT. When returning to our Figure 9, the IRC from Swarm A (top row) also show the typical tidal features during daytime, but nothing after sunset. Conversely, the dual-SC IRC (bottom row) provide no indication of tidal activity at all within the latitude range of ±5° MLat. From this comparison in Figure 9 we are inclined to conclude that the tidal signatures reported by Park et al. (2010) are caused by a cross-talk from the EEJ and are not a feature of the F-region current system.

So far, we have shown the advantages of the dual-SC over the single-satellite current estimate approach. But, also the Swarm dual-SC current estimates have their limitations. An important assumption is the high precision of intercalibration between the involved spacecraft Swarm A and C. As mentioned before, this process is much complicated by the thermomagnetic effect and the failure of the ASM on Swarm C.

Efforts for determining systematic biases between the two spacecraft have been described in Section 3.4. Figure 10 reveals in the right column some persistent features, for example, positive values around 05:00 and 18:00 MLT in the northern hemisphere and around noon in the southern hemisphere. For interpreting them in terms of calibration deficits we have to go back to Equation 6.29 Lühr et al. (2020) have provided in their Section 6.5 a detailed assessment of the dual-SC current uncertainties. They show, only biases in the along-track magnetic field component (almost identical to *Bx*) contribute to errors of the current density. Biases in the *By* component cancel since differences of those values, only separated by 5 s, are considered. And *Bz* is not needed at all.

For a quantitative assessment of biases between the two Swarm spacecraft we make use of Equation 6.29 in Lühr et al. (2020). Modified to serve our purposes it reads:

$$\Delta j_z = \frac{\Delta B_x}{\mu_0 \, dl_2} \tag{4}$$

where dl_2 is the spacecraft separation in east-west direction. This value changes with latitude as $dl_2 = 1.4° \cos(\beta) \cdot 111$ km, where β is latitude. The values for Δj_z we can read from the differences between ascending and descending orbital arcs for the dual-SC approach, as shown in the right frames in Figure 10. The Equation 4 can be solved for estimating the bias in ΔB_x between Swarm A and C:

$$B_{x_C} - B_{x_A} = -\Delta j_z \, \mu_0 \cdot 1.4 \cdot \cos(\beta) \, 111 \cdot 10^3 \tag{5}$$

Any resulting magnetic field value is interpreted as a persistent bias, fixed in spacecraft frame, of Swarm C. Equation 5 can be applied to the derived current differences presented in the right frames of Figure 10, and the bin averages of the right column can be further processed as:

$$B_{x_C} - B_{x_A} = -\Delta j_z \, 4\pi \cdot 1.4 \cdot \cos(\beta) \cdot 111 \cdot 10^{-4} \tag{6}$$

When Δj_z is inserted in nA/m^2 the field bias results in nT. The distribution of the spacecraft-fixed ΔB_{xC} is shown in Figure 11, separately for the two seasons. Overall, the mean biases are small, staying below 1 nT, which is the specified value for the field accuracy. Still, systematic patterns appear. A common feature is the negative field in the 04:00–07:00 MLT sector, more prominent in the northern hemisphere. Otherwise, quite different distributions of the ΔB_{xC} biases are derived for the two seasons. During May to Oct., positive values reaching 1 nT (pointing in along-track direction) are outstanding in the northern hemisphere around noon. Interestingly, at the equator they switch to negative values, reaching 0.4 nT in the southern hemisphere. Overall, the ΔB_{xC} biases in in the southern hemisphere are less structured. During Dec. to March., large negative biases are found again around the 05:00 MLT sector, and the positive ΔB_{xC} around noon has been confined to latitudes above 35° Mlat, while stronger negative ΔB_{xC} are found here in the southern low and middle latitudes.

A positive fact to be noted here, spacecraft-fixed biases tend to compensate each other when averaged over equal amounts of ascending and descending orbit arcs. This should be well achieved within the considered 5-year period. Therefore, the obtained fixed biases can only have negligible effect on the presented IHFACs and IRC results near the equator. Still, there seem to be other biases, for example, in the early morning (see Figure 6, 4–6 MLT, Descending), that cause spurious current signatures.

At this point it is not clear, whether imperfections in the corrections of the thermomagnetic effect or in the transfer of the total field value from Swarm A to Swarm C are the reasons for the derived spacecraft-fixed biases, reaching up to 1 nT. It may, however, be noted, at the magnetic equator the *Bx* component is practically identical to the total field. If the field magnitude was correct at both spacecraft, the sudden changes in ΔB_{xC} at the equator should not appear in Figure 11. Based on these results more efforts in calibration are encouraged to address the remaining issues.

5. Summary

In this study we have performed a detailed analysis of the radial (IRC) and inter-hemisphere currents (IHFAC) at equatorial and low latitudes, respectively, derived from the single-satellite and dual-SC approaches of the Swarm satellites. The main findings are summarized as:

1. In most cases, the IRCs and IHFACs derived from both approaches show consistent latitudinal profiles. However, there are certain events with discrepancy exceeding 5 nA/m^2 between two approaches.
2. On average, the diurnal variations of IHFACs from both approaches agree well with each other in all seasons, but the amplitudes from single-satellite amount only to about 70% of those from the dual-SC. Such a difference is caused by the fact that only the magnetic field *By* component is utilized in the single-satellite approach, while there are also significant *Bx* contributions at low and middle latitudes. The dual-SC approach considers both *Bx* and *By* components.

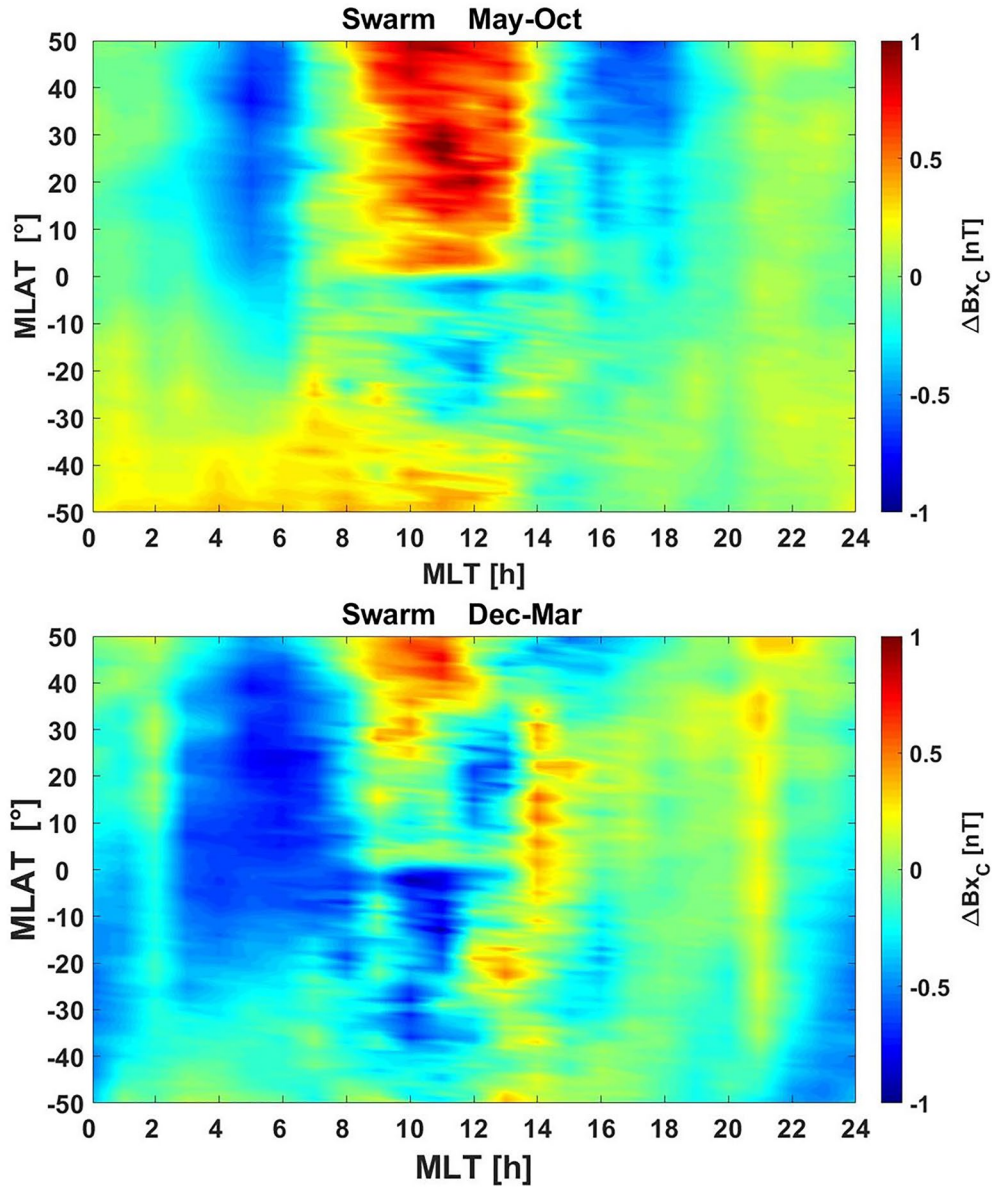

Figure 11. Magnetic latitude versus magnetic local time distributions of ΔB_x estimated from the discrepancy of ionospheric radial currents from dual-SC approach during ascending and descending orbits. Results are presented separately for our two seasons. Positive and negative values of ΔB_x represent error fields of Swarm C directed northward and southward, respectively.

3. Above the magnetic equator, the IRCs derived from single-satellite approach show clear tidal signatures, while such signature cannot be found in the IRCs from dual-SC approach. We interpret the tidal-signature in IRCs from single-satellite as spurious, being due to contributions to the ΔB_y component from the EEJ. Conversely, remote currents have no influence on the dual-SC approach.
4. The dual-SC derived IRCs show notable differences at low and middle latitudes between ascending and descending orbital arcs. Such a differences might be due to violation of the assumption that both Swarm spacecraft are perfectly calibrated. When looking at the differences between up-leg and down-leg orbits we identify systematic spacecraft-fixed biases in the along-track magnetic field component (*Bx*) between Swarm A and C. By attributing all the IRC differences to Swarm C a magnetic biases of ΔB_{xC}, reaching 1.0 nT, are derived.

Our results show that the dual-SC derived currents are in general better suited for revealing the ionospheric current distributions. But a comparison to the single-satellite current estimates can help to identify weaknesses of the dual-SC approach.

Data Availability Statement

The authors want to thank the Swarm team for providing the data at ESA's website: https://earth.esa.int/web/guest/swarm/data-access.

Acknowledgments
This work is supported by the National Natural Science Foundation of China (42174191 and 42174186). Chao Xiong is supported by the Special Found of Hubei Luojia Laboratory (220100011), start-up program of Wuhan University, as well the Dragon 5 cooperation 2020–2024 (project no. 59236).

References

Alken, P. (2020). Estimating currents and electric fields at low latitudes from satellite magnetic measurements. In *Ionospheric multi-spacecraft analysis tools*, (Vol. 17, pp. 233–254). Springer International Publishing. https://doi.org/10.1007/978-3-030-26732-2

Brauer, P., Merayo, J. M. G., Thamm, H., Tøffner-Clausen, L., Amann, M., Hulot, G., et al. (2018). Magnetic perturbations from thermoelectric currents in Swarm thermal blankets. *Geophysical Research Abstracts*, *20*, 5110.

De Michelis, P., Tozzi, R., & Consolini, G. (2017). Statistical analysis of geomagnetic field intensity differences between ASM and VFM instruments onboard Swarm constellation. *Earth Planets and Space*, *69*(1), 1–17. https://doi.org/10.1186/s40623-016-0583-1

Dunlop, M. W., Yang, J.-Y., Cao, J.-B., Fu, H.-S., Yang, Y.-Y., Lühr, H., et al. (2015). Multispacecraft current estimates at swarm. *Journal of Geophysical Research A: Space Physics*, *120*(10), 8307–8316. https://doi.org/10.1002/2015JA021707

Friis-Christensen, E., Lühr, H., Knudsen, D., & Haagmans, R. (2008). Swarm—An Earth observation mission investigating geospace. *Advances in Space Research*, *41*(1), 210–216. https://doi.org/10.1016/j.asr.2006.10.008

Jager, T., Leger, J. M., Fratter, I., Lier, P., & Pacholczyk, P. (2016). *Magnetic cleanliness and thermomagnetic effect: Case study of the absolute scalar magnetometer and its environments on SWARM satellites* (pp. 1–6). Proc. ESA Workshop Aerosp.

Lühr, H., Kervalishvili, G., Rauberg, J., & Stolle, C. (2016). Zonal currents in the F region deduced from Swarm constellation measurements. *Journal of Geophysical Research A: Space Physics*, *121*(1), 638–648. https://doi.org/10.1002/2015JA022051

Lühr, H., Kervalishvili, G. N., Stolle, C., Rauberg, J., & Michaelis, I. (2019). Average Characteristics of Low-Latitude Interhemispheric and F Region Dynamo Currents Deduced From the Swarm Satellite Constellation. *Journal of Geophysical Research: Space Physics*, *124*(12), 10631–10644. https://doi.org/10.1029/2019JA027419

Lühr, H., & Manoj, C. (2013). The complete spectrum of the equatorial electrojet related to solar tides: CHAMP observations. *Annales Geophysicae*, *31*(8), 1315–1331. https://doi.org/10.5194/angeo-31-1315-2013

Lühr, H., Ritter, P., Kervalishvili, G., & Rauberg, J. (2020). *Applying the dual-spacecraft approach to the Swarm constellation for deriving radial current density*. In *Ionospheric multi-spacecraft analysis tools*, (Vol. 17, pp. 117–140). Springer International Publishing. https://doi.org/10.1007/978-3-030-26732-2

Park, J., Lühr, H., & Min, K. W. (2010). Characteristics of F-region dynamo currents deduced from CHAMP magnetic field measurements. *Journal of Geophysical Research*, *115*(10). https://doi.org/10.1029/2010JA015604

Park, J., Lühr, H., & Min, K. W. (2011). Climatology of the inter-hemispheric field-aligned current system in the equatorial ionosphere as observed by CHAMP. *Annales Geophysicae*, *29*(3), 573–582. https://doi.org/10.5194/angeo-29-573-2011

Park, J., Yamazaki, Y., & Lühr, H. (2020). Latitude dependence of interhemispheric Field-Aligned Currents (IHFACs) as observed by the Swarm constellation. *Journal of Geophysical Research: Space Physics*, *125*(2), 1–14. https://doi.org/10.1029/2019JA027694

Rishbeth, H. (1971). The F-layer dynamo. *Planetary and Space Science*, *19*(2), 263–267. https://doi.org/10.1016/0032-0633(71)90205-4

Ritter, P., Lühr, H., & Rauberg, J. (2013). Determining field-aligned currents with the Swarm constellation mission. *Earth Planets and Space*, *65*(11), 1285–1294. https://doi.org/10.5047/eps.2013.09.006

Tøffner-Clausen, L., Lesur, V., Olsen, N., & Finlay, C. C. (2016). In-flight scalar calibration and characterisation of the Swarm magnetometry package. *Earth Planets and Space*, *68*(1), 1–13. https://doi.org/10.1186/s40623-016-0501-6